NeuroImage 185 (2019) 129–139

Contents lists available at ScienceDirect

NeuroImage

journal homepage: www.elsevier.com/locate/neuroimage

How minimal variations in neuronal cytoskeletal integrity modulate cognitive control

Christian Beste [a,*,1], Ann-Kathrin Stock [a,1], Nicolas Zink [a], Sebastian Ocklenburg [b], Katja Akgün [c,2], Tjalf Ziemssen [c,2]

[a] Cognitive Neurophysiology, Department of Child and Adolescent Psychiatry, Faculty of Medicine of the TU Dresden, Dresden, 01307, Germany
[b] Institute of Cognitive Neuroscience, Biopsychology, Department of Psychology, Ruhr University Bochum, Universitätsstrasse 150, 44780 Bochum, Germany
[c] Center of Clinical Neuroscience, Neurological Clinic, University Clinic Carl Gustav Carus, Faculty of Medicine of the TU Dresden, Dresden, 01307, Germany

ARTICLE INFO

Keywords:
Neurofilaments
Cognitive control
Theta oscillations
Networks
EEG

ABSTRACT

Until recently, investigating microscopic changes in the integrity of human brain matter has not been possible in vivo. It has hence remained unknown whether and how small non-pathological variations in cytoskeletal neuronal integrity affect human cognitive functioning. We investigated the role of neuronal cytoskeleton integrity for complex multicomponent behavior, which is relevant to real-life situations, as complex goals are often achieved by assembling a series of sub-tasks. For this, we quantified scaffolding proteins (i.e. neurofilament light; NF-L) using a single-molecule array (SIMOA), a new and uniquely ultra-sensitive method, and integrated this with behavioral and neurophysiological (EEG) data. For the first time, we showcase that slightest non-pathological variations in cytoskeletal integrity strongly modulate the efficiency of cognitive control processes. We show that the architecture and efficiency of theta-oscillations networks during cognitive control processes reflects a mechanism that establishes the relationship between neuronal cytoskeleton integrity and multicomponent behavior. Attentional selection processes do however not seem to play a role. The efficiency and network architecture of theta oscillations provides an important missing neural link that helps to explain how diffuse and seemingly miniscule variations in neuronal integrity may lead to reduced or even impaired cognitive functioning that is important for everyday activities.

1. Introduction

In real-life situations, behavioral goals are often achieved by assembling a series of sub-tasks (Diamond, 2013; Duncan, 2010). For example, steering and switching gears of a car depend on a complex coordination of actions. This sort of behavior has also been referred to as 'multi--component' behavior and is often defined as the ability to interrupt, generate, process, and execute/cascade separate task goals and responses in an expedient temporal order to produce efficient goal-directed behavior (Dippel and Beste, 2015; Duncan, 2010; Mückschel et al., 2014; Stock et al., 2014a). Among other factors, the complexity of multi-component behavior depends on whether the requirement for different actions/task goals is signaled at the same time, or whether there is a temporal gap between stimuli signaling/initiating two (or more) different actions (Dippel and Beste, 2015; Gohil et al., 2016, 2015; Letzner et al., 2017; Mückschel et al., 2014). In case of simultaneous input, one is left with the choice of how to process the different actions/task goals: The two actions could either be processed at once, or be prioritized (i.e. performed in a serial, step-by-step fashion). Because response selection depends on a restricted resource (Meyer and Kieras, 1997; Verbruggen et al., 2008; Wu and Liu, 2008; Wu et al., 2017), this choice directly affects the efficacy of multi-component behaviour. If participants choose to simultaneously process two (or more) task goals, reaction times will increase because these processes have to share a limited capacity (Miller et al., 2009; Verbruggen et al., 2008). If they however choose a more serial step-by-step strategy and prioritize one action over the other, the different actions will not have to share limited response selection capacities so that multi-component behavior becomes

* Corresponding author. Cognitive Neurophysiology, Department of Child and Adolescent Psychiatry, Faculty of Medicine of the TU Dresden, Schubertstrasse 42, D-01309 Dresden, Germany.
E-mail address: christian.beste@uniklinikum-dresden.de (C. Beste).
[1] Contributed equally as first authors.
[2] Contributed equally as senior authors.

https://doi.org/10.1016/j.neuroimage.2018.10.053
Received 9 May 2018; Received in revised form 13 October 2018; Accepted 19 October 2018
Available online 19 October 2018

more efficient (i.e. faster). Following from this, the efficiency of multi-component behavior can be assessed by comparing the behavioral performance in a "baseline" condition with enforced serial processing to a condition that leaves a free choice of how task goals are processed. In this setting, slower responses in the latter condition indicate less expedient multicomponent behavior (Mückschel et al., 2015, 2014; Stock et al., 2014a).

Multi-component behavior can be seen as the result of information integration in a wide-spread functional neuroanatomical and neurophysiological network (Brandt et al., 2017; Duncan, 2010; Gohil et al., 2015; Mückschel et al., 2014; Stock et al., 2017). On a neural network level, the most efficient way to build a robust scalable network is through predominantly local wiring (Van Essen, 1997). In this case, brain structures receive most information from their immediate neighbors and act locally, as communicating with distant neurons via interneurons is metabolically expensive (Kalisman et al., 2005). Yet, a neuronal network that enables the brain to perform a complex coordination of several task goals or actions (i.e. multi component behavior) must not only exhibit a high local information processing efficiency, but also a high global information processing efficiency. Networks which accomplish both exhibit so-called "small-world properties" (Achard and Bullmore, 2007; Bassett and Bullmore, 2006; Bullmore and Sporns, 2009), which are thought to enable the efficient separation *and* functional integration of information (Achard and Bullmore, 2007; Bassett and Bullmore, 2006). According to the temporal binding hypothesis (Crick and Koch, 2003; Varela, 1995; von der Malsburg, 1994); the communication of two distant neural populations cannot be explained by anatomical connectivity per se but rather by the coherent temporal organization of activity through oscillatory synchrony (Buzsáki, 2006; Buzsáki and Draguhn, 2004). This "binding by synchrony" mechanism emphasizes the importance of the oscillatory phase in the pairing of distinct neuron assemblies and explains how many signals may be transmitted in parallel without interference (Buzsáki, 2006; Varela, 1995). From a biophysical point of view, it has been shown that low-frequency/high-amplitude neural oscillations in neural networks reflect an ideal scheme to organize activities across large spatial distances and brain regions (Buzsáki, 2006). This may particularly be the case for medial frontal theta oscillations (Cavanagh and Frank, 2014) and could be one of the reasons why theta frequency oscillations play a key role in mediating cognitive control (Cavanagh and Frank, 2014; Cohen, 2014). Theta oscillations are also important for information integration in more circumscribed neural assemblies during cognitive control (Cohen, 2014). This implies that theta oscillations likely serve both large-scale and small-scale information integration in a neuronal network and could be considered an information coordination mechanism within a small-world-like network organization. It is therefore likely that the ability to efficiently accomplish multi-component behavior relates to strong small-world properties. Due to these considerations, especially the small-world metric may be particularly suitable to examine the network architecture during cognitive control using neurophysiological (EEG) methods. Regarding neurophysiological (EEG) methods, it is important to consider that the EEG signal depends on the transient synchronization of local field potentials (Hipp et al., 2012; Pfurtscheller and Lopes da Silva, 1999). Importantly, the conceptualization of small-world networks and the mechanism underlying the connection of neural assemblies is also based on the transient synchronization of local field potentials (Achard and Bullmore, 2007; Bassett and Bullmore, 2006). Thus, the small world measure is based on properties also constituting the EEG signal. This makes the small-world metric particularly suitable to characterized EEG networks (Vecchio et al., 2018).

On a molecular level, a natural limiting factor for information integration in such a network is the constitution of the neuronal cytoskeleton, which is determined by scaffolding proteins; i.e. intermediate filaments (Lariviere and Julien, 2004; Lépinoux-Chambaud and Eyer, 2013; Zetterberg et al., 2013). Neurofilament (NF) proteins, especially the neurofilament light (NF-L), which is a protein that is abundantly expressed in long myelinated subcortical white matter axons (Zetterberg et al., 2013), constitute the major intermediate filament type in adult neurons. The NF-L subunit serves as the core of the neurofilament protein and regulates neuronal differentiation (Kong et al., 1998; Zetterberg et al., 2013). Neurofilaments (especially the heavy chain of NF) are of essential importance for the structural integrity and thereby the conduction velocity of nerve impulses (Kriz et al., 2000), which constitute the basis for any electrophysiological network. Under healthy conditions, NF-L shows close relations with the integrity of the brain parenchym (Vågberg et al., 2015). Following axonal damage or dysfunction, NF-L leaks into the interstitial (cerebrospinal) fluid and subsequently into the bloodstream, where it can be detected and measured in serum samples (sNF-L) correlating with in-time NF-L CSF release (Disanto et al., 2017, 2016; Teunissen and Khalil, 2012). Notably, there are close links between NF-L and the integrity of white matter structure as shown in studies on demyelinating diseases (Boesen et al., 2018; Khalil et al., 2018; Kuhle et al., 2016b, 2017; Melah et al., 2016) and structural imaging studies on longitudinal white matter degeneration (Racine et al., 2017). The white matter connectivity pattern and the integrity of this has also been shown to alter the dynamics of scalp EEG signals (Gong et al., 2017). The relevance of structural (white matter) connectivity for EEG scalp signal network dynamics seem to be that important, that the inter-relation of these measures is discussed to be of clinical diagnostic relevance (Teipel et al., 2016). It is therefore possible that neurobiological elements (i.e. scaffolding proteins) affect neurophysiological network properties, as measured using EEG methods while participants engage in cognitive control functions. Importantly, using a single-molecule array (SIMOA) assay, it is possible to estimate the concentration of NF proteins at concentrations as low as 10–20 molecules/100 µl (i.e. concentrations $<10^{-15}$ M) (Kuhle et al., 2016c) in blood sera (Disanto et al., 2017). SIMOA has a 126- and 25-fold higher sensitivity than the ELISA and ECL assays, respectively. It has furthermore a lower limit of quantification of 0.0178 pg/ml (Gisslén et al., 2016; Kuhle et al., 2016a). It is therefore possible to investigate the effects of even the slightest variations in the constitution of the neuronal cytoskeleton on measures of cognitive control and multi-component behavior. Given that both the structural integrity of the neuronal cytoskeleton and theta oscillations are pivotal for the coordinated and expedient processing of complex input, we further hypothesized that these factors should not only be closely linked to the efficacy of multi-component behavior, but should also be closely associated with one another. Specifically, we hypothesized that the architecture and efficiency of theta-oscillation based networks reflects a mechanism that establishes the relationship between microscopic (structural integrity of the neuronal cytoskeleton) and macroscopic aspects (multi-component behavior performance) in the coordination of complex actions.

To investigate these hypotheses, we examined the modulation of cognitive control and multi-component behavior by normal, non-pathologic molecule-level variations in scaffolding proteins (i.e. sNF-L). Healthy young adults performed a stop-change paradigm (Mückschel et al., 2014; Verbruggen et al., 2008) that requires fast and comparatively easy right hand GO responses in two thirds of trials, while one third of the trials requires stopping the right hand GO response (just like in a stop-signal task) and additionally changing to an alternate left hand response (so-called stop-change or SC trials). By varying the time interval between STOP and CHANGE stimuli it is possible to scale the difficulty to execute a correct response on the CHANGE stimulus. In a "baseline" condition, the time interval forces participants to processes STOP and CHANGE stimuli in a step-by-step fashion. In a "test" condition STOP and CHANGE stimuli are presented simultaneously (SCD0 condition). By calculating a slope value which reflects the response time difference between the two conditions (for details please refer to the methods section), we obtained a single behavioral score which reflects the efficacy of multicomponent behavior. We expected higher sNF-L values to be associated with reduced theta small-world properties and less expedient multicomponent behavior. Since multi-component behavior as one

instance of cognitive control can be seen as the result of information integration in a wide-spread functional neuroanatomical and neurophysiological network (Duncan, 2010; Gohil et al., 2015; Mückschel et al., 2014; Stock et al., 2017), especially this kind of task may be suitable to examine the relevance of cytoskeletal integrity for cognitive control processes.

2. Materials and methods

A sample of N = 60 healthy, young human participants (19–32 years, mean age 24.17, SD = 3.25; 24 males) took part in the study. All participants were right-handed and had an average education level of 16.4 ± 3.1 schooling years. All subjects had normal or corrected-to-normal vision, normal hearing capabilities, and no history of any neurological and psychiatric disorders. The study was approved by the ethics committee of the medical faculty of the Technische Universität Dresden and the Ruhr-Universität Bochum. All subjects provided written informed consent and were treated in accordance with the Declaration of Helsinki. The sample size was estimated a-priori assuming medium to low effect sizes ($f^2 = 0.25$) in the correlation and regression analyses, an alpha error probability of 5% and a power of 95%, we estimated a total sample size using G-Power software (http://www.gpower.hhu.de/) and ended up with a minimum sample size of n = 57 in case of one predictor. Based on this, we decided to include n = 60 individuals in our sample. We had to exclude n = 1 subject from all analyses including sNF-L values because the SIMOA analysis was not possible. All subjects were tested at the same time so that diurnal aspect cannot modulate the pattern of results.

2.1. Task

To examine multi-component behavior and to vary the demands on multi-component behavior, an established Stop-change paradigm was used (Mückschel et al., 2014; Stock et al., 2014a; Verbruggen et al., 2008). In short, this paradigm requires fast and comparatively easy right hand GO responses in two thirds of the trials, while one third of the trials requires stopping the right hand GO response (like in a stop-signal task) and additionally changing to an alternate left hand response. The order of the 864 trials was pseudo-randomized in each of the six experimental blocks. The experimental paradigm is illustrated in Fig. 1.

During the task, the subjects were presented with a white bordered rectangle (55 × 16 mm) on a black background (0.4 cd/m^2) which contained 4 vertically arranged circles with white borders, which were separated by three white horizontal lines (width 13 mm, line thickness 1 mm) (17 inch CRT computer monitor, viewing distance of 57 cm). At the beginning of each trial, this array was presented for 250 ms. Then, one of the four circles (diameter of 7 mm) was filled in with white color (120.1 cd/m^2), thus becoming the target stimulus in the GO condition. This GO stimulus remained on the screen until the end of the trial. The participants were instructed to press one of two keys on the keyboard with their right hand in order to report the location of this GO stimulus in relation to the middle line. Specifically, participants had to respond with their right middle finger ("K" key) when the target was located above the middle line, and to respond with their right index finger ("N" key) when the target was located below the middle line. The participants were asked to respond within 1000 ms after the target stimulus onset. Otherwise, a speed-up sign (the German word "Schneller!" which translates to "Faster!") appeared above the stimulus array. This GO condition was presented in two thirds of the trials presented in the experiment.

The other one third were Stop-Change (SC) trials. These trials also began with the empty array followed by the GO stimulus. However, a STOP stimulus (the white rectangle border turned red, see Fig. 1) was presented after the GO stimulus during these trials. The onset asynchrony between the GO and STOP stimuli was determined by a variable Stop-signal delay (SSD), which was adjusted to each participant's individual task performance. This was done using a staircase algorithm (Verbruggen et al., 2008): Initially, the SSD was set to 250 ms. When the participant did not press a key before the presentation of the STOP stimulus and correctly responded to the CHANGE stimulus as described below, the SSD was increased by 50 ms for the next SC trial. In contrast to this, any incorrect responses during SC trials (i.e. responses within the SSD/before the CHANGE stimulus as well as wrong responses to the CHANGE stimulus) decreased the SSD for the next SC trial by 50 ms. As a result, the staircase procedure produced a 50% probability of successfully performed stopping on SC trials in case participants correctly followed the task instructions. Importantly, the 50% adjustment was only done during

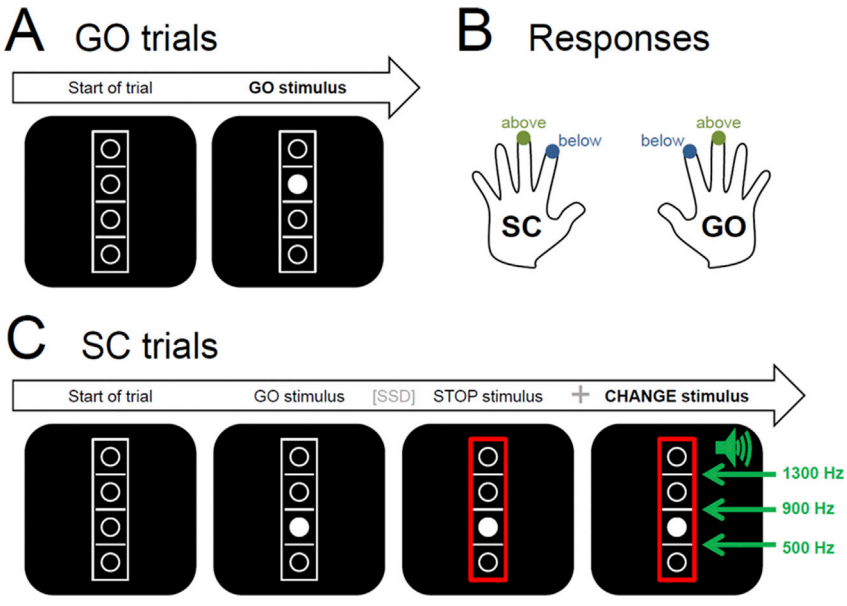

Fig. 1. Illustration of the Stop change task.
In all conditions of this task, the subjects were asked to judge the location of a single target (white filled circle) in relation to either the middle reference line (GO trials, see figure part A) or to the reference line indicated by the CHANGE stimulus (SC trials, see figure part C). Every trial started with a 250 ms presentation of the empty visual array, followed by the target stimulus (white filled circle), which appeared and stayed on the screen until the first given response. (B) In simple GO trials, participants were required to respond with their right hand, while the left hand should be used in Stop-Change (SC) trials. To indicate that the target was located below the respective reference line, the index fingers had to be used. To indicate that the target was located above the respective reference line, the middle fingers had to be used.
(C) All SC trials started like regular GO trials, but an additional stop signal (red frame) was added to the visual array after a variable stop signal delay (SSD). The participants were told to inhibit their right hand response upon the occurrence of the stop signal. The change signal was either presented simultaneously with the stop signal (SCD0 condition), or with a stop-change delay (SCD) of 300 ms (SCD300 condition). In SC trials, participants had to judge the target's position relative to the reference line indicated by the change signal: A binaural high (1300 Hz) tone coded for the high reference line, a medium tone (900 Hz) for the middle line and a low tone (500 Hz) for the low line. Please note that all green annotations are only for illustrator purposes and were not shown to the participants.

the staircase procedure to examine the SSRT; i.e. was related to the STOP stimulus. Performance on the CHANGE stimuli was not adjusted to 50%. The SSD variation was restricted to range from 50 to 1000 ms to keep the trial duration within reasonable limits.

Like the GO stimulus, the STOP stimulus remained on the screen until the participants had responded to the CHANGE signal (a 200 ms sine tone, which was presented via headphones to both ears). In each SC trial, one of three differently pitched tones (low/500 Hz, middle/900 Hz, and high/1200 Hz) was presented at a 75 dB sound pressure level. Prior to the testing, we ensured that each of the different pitches could be discriminated with at least 95% accuracy. The participants were instructed to relate the target stimulus (i.e. the white circle) to the horizontal reference line indicated by the CHANGE stimulus: When the change signal was a low tone, the low line became the new reference line. Following the same logic, the middle tone encoded the middle reference line, while the high tone represented the upper reference line. Participants had to respond with their left hand middle finger ("S" key) whenever the target was located above the newly set reference line and had to respond with their left hand index finger ("C" key) when the target was located below the newly set reference line. If participants did not respond within 2000 ms after the onset of the CHANGE stimulus, the speed up sign appeared above the stimulus array and stayed on the screen until the trial was terminated by a button press. The reaction time (RT) was measured relative to the presentation of this CHANGE stimulus.

Lastly, there were two SC conditions which varied the demands on cognitive processes during multi-component behavior. In the first condition, there was no Stop-Change delay (SCD0) so that STOP and CHANGE stimuli were presented at the same time. The second SC condition had a stimulus onset asynchrony of 300 ms (SCD300) so that the CHANGE stimulus always followed the onset of the STOP stimulus after 300 ms. This important experimental manipulation was implemented for the following reasons: According to the bottleneck model, response selection processes depend on a restricted resource. The simultaneous processing of the STOP and CHANGE in the SCD0 condition imposes high demands on these selection processes, which leads to long RTs (Dippel and Beste, 2015; Mückschel et al., 2014; Stock et al., 2014a; Verbruggen et al., 2008) In the SCD300 condition, demands are comparably lower. Because the STOP and CHANGE processes do not fully overlap in this condition, response selection must occur in a serial/step-by-step fashion (Dippel and Beste, 2015; Mückschel et al., 2014; Stock et al., 2014a; Verbruggen et al., 2008).

2.2. Multi-component behavior mode and efficacy

In the stop-change paradigm outlined above, three task goals have been shown to contribute to the behavioral performance (Verbruggen et al., 2008): (i) responding to the GO signal, (ii) stopping with the stop signal and (iii) responding to the change signal. Importantly, only the SCD0 condition leaves a choice how to process STOP and CHANGE associated processes (i.e. rather serially or in parallel), while the SCD300 condition enforces a rather serial processing because the STOP process is finished by the time the CHANGE stimulus is introduced (Verbruggen et al., 2008). In this context, it is important to consider that response selection is subject to processing capacity limitations. If participants choose to simultaneously process STOP- and CHANGE-associated task goals in the SCD0 condition, reaction times on the CHANGE stimulus increase because the two processes must share a limited capacity. If participants however choose a strategy in which they process STOP- and CHANGE-associated task goals in a rather serial step-by-step manner, the STOP and CHANGE processes do not have to share a limited capacity. This leads to relatively shorter CHANGE RTs in the SCD0 condition than a strategy in which STOP- and CHANGE-associated task goals are processed simultaneously. In other words, multi-component behavior in the highly demanding SCD0 condition becomes more efficient (i.e. CHANGE responses become faster) when a more serial task set processing approach is taken. If an inefficient processing strategy has been used in the SCD0 condition, RTs are substantially longer than in the SCD300 condition, which serves as a "baseline" condition due to the enforced serial processing. If an efficient step-by-step processing strategy has been used in the SCD0 condition, the RT are closer to those of the SCD300 condition. The ratio of RT differences in the SCD0 and SCD300 conditions therefore gives an estimate of an individual's the efficiency during action cascading (Verbruggen et al., 2008):

$$slope = \frac{RT_{SCD0} - RT_{SCD300}}{SCD_{SCD0} - SCD_{SCD300}} = \frac{RT_{SCD0} - RT_{SCD300}}{-300}$$

This slope value is calculated for each participant individually and becomes steeper (i.e. yields more negative values) with increasing RT differences between the two conditions. Therefore, a steeper slope indicates a less efficient multi-component behavior.

2.3. EEG recording and processing

EEG was recorded from 65 Ag—AgCl electrodes using a QuickAmp amplifier (Brain Products Inc.) at standard scalp positions against a reference electrode located at FCz. The sampling rate was 1 kHz, which was down-sampled off-line to 256 Hz. During recording, all electrode impedances were kept below 5 kΩ. Data processing started with the application of a band-pass filter ranging from 0.5 to 18 Hz (48db/oct). This was followed by a manual inspection of the data to remove technical artifacts. To correct for periodically recurring artifacts (pulse artifacts, horizontal and vertical eye movements) an independent component analysis (ICA; Infomax algorithm) was applied to the un-epoched data set. Independent component showing these artifacts were discarded. The number of ICs removed varied between 2 and 5 (mean = 3.2 ± 1.8). Lastly, a second manual raw data analysis was run to remove any residual artifacts and electrode FCz was topographically interpolated. Then, the EEG data was segmented (stimulus-locked) with respect to the onset of the STOP stimulus for the two SC conditions (i.e. SCD0 and SCD300 trials) (Dippel and Beste, 2015; Mückschel et al., 2014; Stock et al., 2014a). Each of the segments started −2000 ms before the onset of the STOP stimulus (set to time point zero) and ended 2000 ms thereafter. The epoch length was chosen to allow a reliable estimation of the power of low frequency (theta) oscillations. Within these segments, an automated artifact rejection procedure was applied. The rejection criteria were a value difference of more than 100 μV in a 200 ms interval, activity below 0.5 μV in a 200 ms interval. The artifact rejection procedure eliminated ~2.5% (±1.2) of all trials, with no statistically significant difference between experimental conditions. To eliminate the reference potential, a current source density (CSD, order of splines = 4, maximum degree of Legendre polynomials = 10, default lambda = 1e-5) transformation was applied (Nunez and Pilgreen, 1991). The CSD transformation works as a spatial filter (Kayser and Tenke, 2015), which reduces the impact of volume conduction. This helps to identify the electrodes that best reflect neurophysiological (EEG) activity related to specific cognitive processes. According to previous work using the same experimental paradigm (Mückschel et al., 2014), a baseline correction was then set to the time window from −900 till −700 ms before STOP stimulus onset to obtain a pre-stimulus baseline that is also prior to the onset of the GO stimulus (which occurred on average 215 ms ± 9 before the STOP stimulus onset, as indicated by the mean SSD). The methods on the add-on analysis of event-related potentials (ERP) and source localization of ERP data is shown in the supplemental material. Using the single-trial, baseline-corrected data obtained after the EEG preprocessing steps, we conducted a time-frequency decomposition applying Morlet wavelets (w) in the time domain to different frequencies (f):

$$w(t,f) = A\,\exp(-t^2/2\sigma_t^2)\exp(2i\pi ft)$$

where t is time, $A = (\sigma_t\sqrt{\pi})^{-1/2}$, σ_t is the wavelet duration, and $i = \sqrt{-1}$. For analysis and TF-plots, a ratio of $f_0/\sigma_f = 5.5$ was used, where f_0 is the

central frequency and σ_f is the width of the Gaussian shape in the frequency domain. The analysis was performed in the frequency range 0.5–18 Hz with a central frequency at 0.5 Hz intervals. The single-trial wavelet-transformed data were subsequently averaged to calculate the total (induced) wavelet power (Roach and Mathalon, 2008), which was quantified at 6 Hz for theta frequency oscillations.

2.4. Small world network analysis

As outlined in the introduction, we focused on the theta frequency band, i.e. on oscillations between 4 Hz and 8 Hz, for the network connectivity analysis. The procedure used to examine network connectivity and small-world network analysis has been used previously in EEG data (Wolff et al., 2017). To examine the 'communication' between all EEG electrodes in terms of a 'network', we assessed the connectivity between the electrodes. This was done using the strength of coherence (Peters et al., 2013; Stam and van Straaten, 2012), which is probably the simplest and most popular measure of "interaction" at a specific frequency (Nunez et al., 1999, 1997). All electrodes were treated as nodes in the network and connections (edges) between these nodes are defined as coherence between all possible pairs of electrodes. For the calculation of the coherence values, only the imaginary part of the coherence spectrum of all possible pairs of nodes was used to effectively suppress spurious coherence driven by volume conduction (Nolte et al., 2004).

This was done for all CSD transformed and segmented single trial data for each condition, which were filtered for theta oscillations between 4 Hz and 8 Hz. The reason for applying this filter is that we were only interested in low-frequency/high-amplitude neural oscillations (i.e. theta oscillations) which were shown to organize activities across large spatial distances and brain regions, especially during cognitive control (Cavanagh and Frank, 2014). While there are several ways to determine the threshold, for instance based on some statistical parameterization or previous observation in the literature, all of them remain arbitrary. The threshold was applied to a matrix containing all (imaginary part of the) coherence values of all single trials. This was done separately for each individual. For the analysis of the coherence values, only the highest 15% of each individual's coherence values were included in the analysis. This approach is a compromise that is made to cope with two problems: On the one hand, it makes sure that only electrodes with high coherence are defined as being "connected" and are included in the analysis. On the other hand, it also makes sure that enough connections are left to still form an electrode connectome which may be considered as a network (Wolff et al., 2017; Zink et al., 2018). A binary 65×65 adjacency network matrix (based on the 65 included electrodes) was then calculated with 1 representing an un-weighted and undirected connection between any pair of electrodes and 0 representing no connection. In order to study small world networks, the method by (Watts and Strogatz, 1998) was applied to each single-subject (Wolff et al., 2017; Zink et al., 2018): Starting from a one-dimensional network, where each node in the network is only connected to its k nearest neighbors on either side, representing a 'regular' network with randomness $\acute{o} = 0$, a ring lattice with N nodes of mean degree $2k$ is created. Next, more connections ('edges') are randomly chosen to another random node with increasing randomness ($\acute{o} > 0$). So, when $\acute{o} = 0$, no edges are rewired and the model returns a ring lattice. In contrast, when $\acute{o} = 1$, all of the edges are rewired and the ring lattice is transformed into a random network with N nodes and mean node degree of $2k$. According to the Watts and Strogatz model, a network has small-world network properties when it demonstrates properties from both lattice networks, with clustered interconnectivity within groups of nodes sharing many nearest neighbors in common (high clustering coefficient, 'C'), and properties from random networks, represented by a short geodetic distance (average path length, 'L') between any two nodes in the network. Thus, the balance of local segregation and global integration in neural networks ('small worldness') can be quantified by C and L, respectively (Bassett and Bullmore, 2006). Regular networks have a high C, but also a very high L. In contrast, random networks have a low C and a low L. Hence, neither regular nor random networks alone can explain the small world phenomenon (Watts and Strogatz, 1998). For each subject, the average number of edges from one node to all other nodes (degree, $2k$), average shortest path length (geodetic distance, L_{real}) and average clustering coefficient (C_{real}) were calculated. Corresponding to each individual's degree, completely random ($\acute{o} = 0$) and completely regular ($\acute{o} = 1$) Watts Strogatz models were created and L_{rand} and C_{rand} and C_{latt} were computed. We analyzed all small world values (ω) according to (Telesford et al., 2011), who proposed a quantitative categorical definition of a small-world network in line with the definitions of the original Watts-Strogatz model. In this way, it can be statistically tested whether a network has small world properties. The small-world value (SWV) formula is expressed by:

$$\omega = \frac{L_{rand}}{L} - \frac{C}{C_{latt}}$$

In the formula, the index "rand" refers to a random network and the index "latt" to a lattice network. Small-world values of ω are restricted to the interval −1 to 1 regardless of network size. If ω is close to zero, it is considered as small world. Positive ω values represent more random properties, negative values indicate that a network has more regular or lattice-like properties. The small-world metric ω (omega) proposed by Telesford et al. (2011) compares network clustering to an equivalent lattice network and path length to a random network, as Watts and Strogatz originally described. In contrast to the standard application, where networks are interpreted as small-world when clustering is compared to a random network, these are not small-world according to ω. The use of ω may prohibit false positives, because Telesford et al. (2011) showed that many systems originally thought to have small-world processing capabilities may in fact not. Furthermore, as outlined in the methods section, positive ω values represent more random properties, whereas negative values indicate that a network has more regular or lattice-like properties. These differential network characteristics cannot be captured by the standard application by Watts and Strogatz, which can only determine whether a network has a more small-world characteristics than others.

2.5. Single molecule array (SIMOA) analysis

After collection, serum samples were stored at −20 °C until neurofilament testing. Neurofilament-light chain (NF-L) measurement was performed using the Simoa Human Advantage NF-Light singleplex Kit and prepared as recommended in the manufacturer's instructions (Quartered, Lexington, MA, Datasheet Quanterix: Simoa™ NF-Light® Advantage Kit). The Simoa Human Advantage NF-L assay is a digital immunoassay for the quantitative determination of NF-L and was ran on a Simoa HD-1 instrument (Quanerix) using a 2-step Assay Neat 2.0 protocol (Wilson et al., 2016). The antibodies and calibrators used in the assays have been developed by Uman Diagnostics (Sweden) and described previously in their plate-based ELISA (Petzold et al., 2010). There are more than 10,000 data points for these ELISAs and the antibodies have been adapted to generate an ultra-sensitive Simoa assay (Kuhle et al., 2016a). These antibodies recognize epitopes in the mid-domain of the NF-L chain. The Simoa NF-L Advantage assay has been validated as fit-for-purpose assay and the lower limit of quantification is 0.0178 pg/ml (Datasheet Quanterix: Simoa™ NF-Light® Advantage Kit). Previous reports proofed that the newly developed single-molecule array (Simoa) technique is the most sensitive opportunity to detect NF-L even in lowest concentrations (Kuhle et al., 2016a). Before starting measurement, 96-well-assay plate was prepared and filled with calibrators, serum samples and controls at room temperature (Quanterix). Capture antibody coated beads, biotinylated detector antibody, streptavidin-beta-galactosidase, resorfurin

beta-D-galactopyranoside and buffers were loaded onto the Simoa HD-1 Analyzer. Assay was run using the 2-step Neat protocol. In the 2-step immunoassay, target antibody coated paramagnetic beads were combined with sample and biotinylated detector antibody in the same incubation step. Target molecules present in the sample were captured by the antibody coated beads and bound with the biotinylated antibody detector simultaneously. Calibrators (8 calibrator points) and diluted serum samples (dilution 1:4) were measured in duplicates. Sample dilution was calculated and done by the instrument. Calibrators ranged from 0 to 500 pg/ml. Predefined control measurements ensured concentration in expected range and proofed validity of the calibration curve and testing procedure.

2.6. Statistics

Separate repeated-measures ANOVAs were used to analyze the behavioral and neurophysiological data. "SCD condition" (SCD0 vs. SCD300) was always used as a within-subjects factor. For the analyses of ERPs, "electrode" was used as an additional within-subjects factor, whenever applicable. Linear correlation analyses and regression analyses were conducted to assess the function nexus between sNF-L values and the RT slope as well as the theta ω slope. Age was included in all regression analyses which yielded significant results. We further used the PROCESS toolbox for SPSS 24 (Hayes et al., 2017) to conduct a mediation analysis with sNF-L and the theta ω slope as potential predictors of the RT slope. All reported results underwent Greenhouse-Geisser correction and post-hoc tests were Bonferroni-corrected, whenever necessary. For all descriptive statistics, the standard error of the mean (SEM) is given as a measure of variability.

3. Results

3.1. Lower sNF-L concentrations are associated with more expedient behaviour

As done in previous studies using the stop-change paradigm, we focused our behavioral analysis on response times (RTs) in correct trials (Mückschel et al., 2014; Stock et al., 2014a). In the task, participants were required to interrupt an ongoing response in a third of trials and change to an alternative response. In the other trials a simple choice response was required that was not interrupted by a STOP stimulus.

The mean and the standard error of the mean (SEM) are given for the descriptive statistics in the entire results section. The mean reaction time in simple GO trials was 494 ms (±12). The mean stop signal delay (SSD, i.e. the variable delay between GO and STOP stimulus onset in SC trials) was 215 ms (±9) and the mean stop signal reaction time (SSRT) was 223 ms (±17). The SSRT was measured according to Logan et al. (1984), whose method was also used in the original publication of this task (Verbruggen et al., 2008). Importantly, the SSRT is shorter than the stop-change delay in the SCD300 condition, which demonstrates that the STOP process was indeed finished before the CHANGE stimulus was presented. This proves that a step-by-step processing of task goals was indeed enforced in the SCD300 condition (Verbruggen et al., 2008). Furthermore, the RTs of CHANGE responses were on average significantly shorter in the SCD300 condition (893 ms ± 25) than in the SCD0 condition (1073 ms ± 23) ($t(59) = 22.82$; $p < .001$). The slope of the SCD-RT function, which reflects the RT difference between the two SCD condition was −0.59 (±0.02), which is in line with previous results (Mückschel et al., 2014; Stock et al., 2014a; Verbruggen et al., 2008). A high slope value indicates that response selection on CHANGE trials is less efficient, because subjects with a high slope value try to process STOP and CHANGE task goals in "parallel". A smaller slope value shows that even in the SCD0 condition subject tend to process STOP and CHANGE processes separately (in a "step-by-step", serial fashion), even though both stimuli are presented at the same time. The distribution of the slope value is shown in supplementary Figure 3.

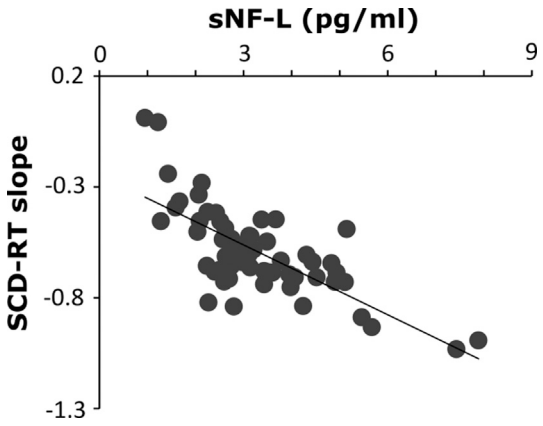

Fig. 2. Correlation between sNF-L levels and behavioral performance. Serum concentrations of neurofilament light (sNF-L) are given on the x-axis in pg per ml, with larger values indicating reductions in neuronal cytoskeleton integrity. The slope of the SCD-RT function is provided on the y-axis, with larger (i.e. more negative) values indicating reductions in the efficacy of multicomponent behavior. As indicated by the regression line, behavioral performance decreased with increasing sNF-L levels.

The mean sNF-L level was 3.31 pg/ml (±0.18), which is in line with other studies in healthy samples (Disanto et al., 2016; Gaiottino et al., 2013). In line with the hypothesis, a correlation analysis revealed a positive correlation between our subjects' sNF-L concentrations and their behavioral slope value, i.e. lower sNF-L levels were correlated with a flatter slope of the SCD-RT function ($r = 0.660$; $R^2 = 0.43$; $p < .001$) (refer Fig. 2).

Given that sNF-L levels increase with age (~2.2% in each year) (Disanto et al., 2017; Vågberg et al., 2015), we also examined whether age affected the observed correlation. Using "age" in a linear regression model, we found that the factor age was not a significant predictor of performance ($t = 0.54$; $p > .4$), while "sNF-L level" remained predictive of the slope value ($t = 6.63$; $p < .001$) ($F(2,56) = 43.96$; $p < .001$). Since sNF-L data collection and the other experimental procedures testing were always carried out at the identical time, circadian rhythms cannot affect the results.

3.2. The architecture of theta-oscillation networks establishes the nexus between sNF-L concentrations and behavioral performance

The P3 ERP component, which has been shown to reflect behavioral inhibition and change processes in the stop-change paradigm (Dippel and Beste, 2015; Mückschel et al., 2014; Stock et al., 2014a), is shown in Fig. 3A.

The statistical analysis (refer supplementary material) revealed no correlations with sNF-L data (all $r < 0.095$; $p > .3$) and replicated the results of previous studies on SCD condition effects (refer supplementary material). However, the main neurophysiological focus of this study were modulations of theta oscillations: The time-frequency plots for electrode Cz are shown in Fig. 3B. A dependent samples *t*-test for the theta frequency power at 6 Hz in SC trials showed that theta frequency power was higher in the SCD0 condition (3.86 ± 0.02) than in the SCD300 condition (3.66 ± 0.02) ($t(59) = 6.94$; $p < .001$). Theta power was not correlated with sNF-L levels (all $r < 0.195$; $p > .3$). As outlined in the introduction and methods sections, the small world value (ω) (Telesford et al., 2011) provides information about the architecture of theta oscillation network. The network plots of theta frequency oscillations in the SCD0 and the SCD300 condition are shown in Fig. 3C. Regarding the small-world values (ω) in the theta frequency band, we found larger ω (i.e. less small-world like) values in the SCD0 condition (0.67 ω ± 0.005) than in the SCD300 condition (0.60 ω ± 0.09) ($t(59) = 12.11$; $p < .001$). The small-world values in the SCD0 and the SCD300 condition were not

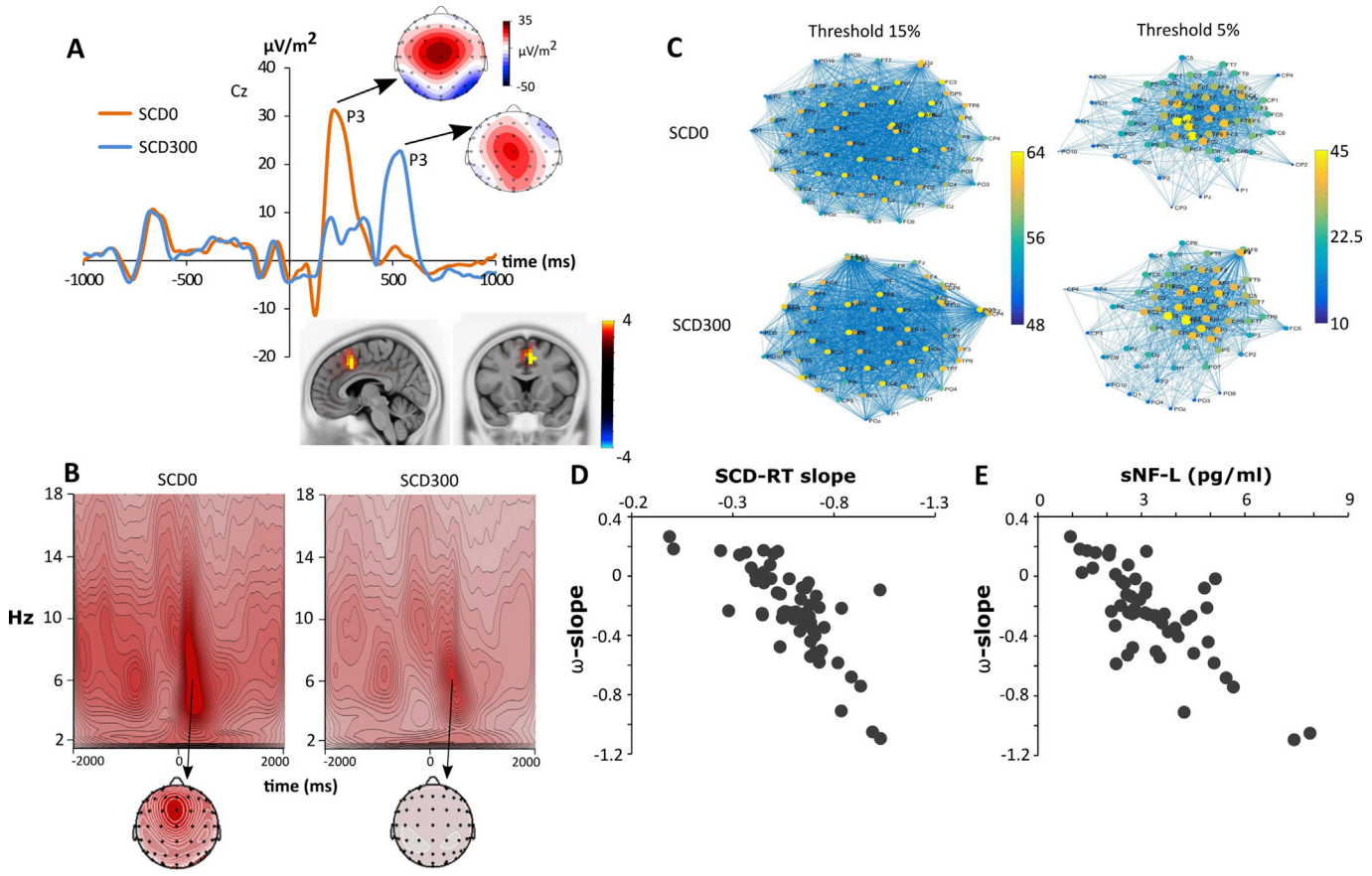

Fig. 3. Neurophysiological correlates of cognitive control and their relation to behavioral and sNF-L data.
(A) The P3 ERP component at electrode Cz is shown for the SCD0 condition (orange) and the SCD300 condition (blue). Time point zero denotes the time point of STOP stimulus presentation. Please note that the onset of the CHANGE stimulus was at time point 0 in the SCD0 condition and at 300 ms in the SCD300 condition. The scalp topography plots are given for the P3 peak in each condition (red colours denote positive values, blue colours denote negative values). The sLORETA plots show the source of condition-driven P3 amplitude differences (SCD0 > SCD300) in the medial frontal cortex (colour bar denotes critical t-values corrected for multiple comparisons). Even though this ERP has repeatedly been shown to reflect behavioral performance differences in the stop-change task, it was not related to sNF-L levels. (B) Time frequency plots showing the total power in the SCD0 and the SCD300 condition. The red-shadings denote the strength of the power. Stronger fronto-central theta activity was evident in the SCD0 condition. Yet, the power of theta oscillations was also not related to sNF-L levels. (C) Theta oscillation networks for the different experimental conditions (SCD0 and SCD300). The imaginary part of the coherence is plotted as edges between the electrodes (nodes). The colour bar denotes the strength of the imaginary part of the coherence. The networks are shown for two thresholds indicating the 15% strongest connections (threshold 85%) and the 5% strongest connections (threshold 95%). Please note that the graph is not based of the traditional "topographic" map. Instead, the location of single electrodes vary (dependent on the results). The reason why there are so many interconnections in the plot is that these network represent the group mean of a condition. If for instance subject A has a weakly interconnected electrode X (e.g. it only has connections to two other electrodes) and subject B has a very highly interconnected electrode X (e.g. it has connections to 60 other electrodes), the mean connectivity of electrode X to other electrodes can become higher, the more subjects are included in the analysis. Individual connectivity plots are therefore much less interconnected and the many connections emerge because the group mean is shown. (D) Scatterplot showing the correlation between the slope of the SCD-RT function and the slope in parameter ω. (E) Scatterplot showing the correlation between serum concentrations of neurofilament light (sNF-L) and the slope in parameter ω.

significantly correlated ($r = 0.009$; $p > .472$)[3]. There was also no significant correlation between small world values (ω) and the power of theta oscillations in the SCD0 and the SCD300 conditions ($r = 0.11$; $p > .50$). The degree of change in ω (i.e. the slope of ω between the two SCD conditions, which was formed in the same way as the behavioral slope value) was correlated with the slope of the behavioral SCD-RT function ($r = 0.769$; $R^2 = 0.59$; $p < .001$) (refer Fig. 3D). The distribution of the slope value for small world values (ω) is shown in supplementary Figure 3. As can be seen in Fig. 3D, a smaller slope (i.e. a difference between SC conditions) in parameter ω was associated with a smaller slope in the reaction time data (i.e. more expedient multicomponent behavior). Importantly, sNF-L levels were correlated with the slope of ω ($r = 0.758$; $R^2 = 0.56$; $p < .001$) (Fig. 3E): The smaller sNF-L levels, the smaller the decrease in small-world-ness (i.e. the increase in the ω value) from the SCD300 to the SCD0 condition. Together, sNF-L level, behavioral performance (reflected by the RT slope value) and the architecture of the theta oscillation network (reflected by the ω slope value) show close inter-correlations. We therefore calculated a linear regression model to account for these inter-dependencies. Following the suggestions by (Hayes et al., 2017), we used the PROCESS toolbox for SPSS 24 which also allows conducting a mediation analysis to test the hypothesis that the neurophysiological network architecture reflects an underlying

[3] It needs to be stressed that the small-world parameter is shown to be a considerable reliable parameter in the current study. We assessed this aspect by calculating the values only over 'odd' trial numbers and 'even' trial numbers. There was no difference between these values ($p > .6$) and the values were highly correlated ($r = 0.852$; $p > .001$). This shows that even though the provided ω values are point measurement, they are likely to present reliable estimates of the true values. This is further corroborate by the small SEMs for the ω values.

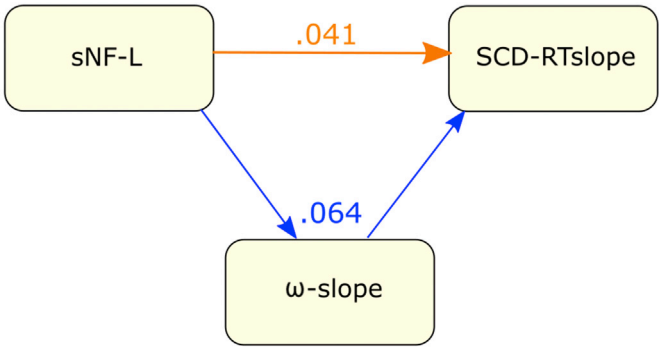

Fig. 4. Results from the statistical mediation analysis.
The interrelation of sNF-L level, the slope of the SCD-RT function and the slope in parameter ω are shown. There is a direct effect of sNF-L levels on the slope of the SCD-RT function (orange line), but also an even stronger indirect effect (blue line), which is mediated by the parameter ω slope. The scatterplots show the correlations.

mechanism via which molecule-level variations in axonal integrity and the neuronal cytoskeleton affect the efficiency of multi-component behavior (refer Fig. 4).

Calculating the linear regression model with sNF-L level and the slope of ω as predictors of the slope of the SCD-RT function revealed a significant regression model ($F(2,56) = 59.85$; $p < .001$; $R^2 = 0.68$; MSE = 0.012). Within this model, both sNF-L ($b = 0.041$; $t = 2.44$; $p = .017$; 95% confidence bounds = 0.007 till 0.073 [2000 bootstrap samples]) and slope of ω ($b = 0.39$; $t = 5.11$; $p < .001$; 95% confidence bounds = 0.239 till 0.548 [2000 bootstrap samples]) were shown to be significant predictors of the SCD-RT slope. There was evidence for a direct effect of sNF-L levels on the slope of the SCD-RT function (effect = .041; 95% confidence bounds = 0.007 till 0.073 [2000 bootstrap samples]. Importantly, there was also evidence for an indirect effect of sNF-L levels on the slope of the SCD-RT function (effect = .064; 95% confidence bounds = 0.038 till 0.086 [2000 bootstrap samples], showing that the slope of ω significantly mediated the effects of sNF-L levels on the slope of the SCD-RT function (refer Fig. 4). Of note, the indirect effect was larger than the direct effect. When using "age" as an additional variable in the mediation analysis (similar to the analysis of the behavioral data), the inclusion of this variable did not change the pattern of results.

Further analyses underline the specificity of these results. We further examined small world network characteristics in the alpha frequency band (i.e. between 8 and 12 Hz) (refer supplemental Figure 1). Modulations in the alpha frequency band are known to be related to variation in P1 and N1 ERPs indexing attentional selection processes (Freunberger et al., 2008; Herrmann and Knight, 2001; Luck and Kappenman, 2013). The small-world value (ω) did not differ between the SCD0 condition ($0.57\ \mu V/m^2 \pm 0.09$) and the SCD300 condition ($0.59\ \mu V/m^2 \pm 0.07$) ($t(59) = -0.98$; $p > .3$). There were also no correlations between the slope of ω in the alpha frequency band and the slope of the SCD-RT function ($r = -0.05$; $p > .70$) or sNF-L levels ($r = -0.12$; $p > .56$). In line with this, we did also not find any correlations of the P1 and N1 ERP amplitudes with sNF-L data (all $r < 0.099$; $p > .3$) (see supplementary material for results and supplementary Figure 2). This lack of effects in attention-related measures further underlines the specificity of results for correlates of cognitive control.

4. Discussion

In the current study, we examined the functional relevance of non-pathological, molecule-level variations in the integrity of the neuronal cytoskeleton for multicomponent behavior and the neurophysiological processes that most likely mediate this nexus. Since multi-component behavior as one instance of cognitive control can be seen as the result of information integration in a wide-spread functional neuroanatomical and neurophysiological network (Duncan, 2010; Gohil et al., 2015; Mückschel et al., 2014; Stock et al., 2017), especially this kind of task may be suitable to examine the relevance of cytoskeletal integrity for cognitive control processes. Molecule-level variations in scaffolding proteins (i.e. sNF-L) were assessed with the help of a SIMOA assay and expected to be correlated with behavioral performance measures (i.e. the RT slope value) as well as neurophysiological correlates of cognitive control (i.e. the small-world-ness of theta oscillations, as reflected by the ω slope) (Mückschel et al., 2014; Verbruggen et al., 2008). Specifically, we expected that both the behavioral and neurophysiological measures should be increasingly impaired (i.e. be characterized by steeper slope values) in case of decreasing neuronal integrity (i.e. increased sNF-L values) (Disanto et al., 2016, 2017; Kuhle et al., 2016c; Teunissen and Khalil, 2012).

First and foremost, we found a strong correlation between sNF-L values and the behavioral RT slope values, which explained ~43% of all observed behavioral variation within the sample. It can therefore be rather safely concluded that non-pathological molecule-level variations in the integrity of the neuronal cytoskeleton are a major determinant of at least some aspects of multicomponent behavior. In line with other studies using the stop-change paradigm, we found that responses to the CHANGE stimuli were longer in the SCD0 condition than in the SCD300 condition. This is because two response options simultaneously demand processing resources in the SCD0 condition, but not in the SCD300 condition, where serial task goal processing is enforced by the stop-change delay. The difference between the two SC conditions is reflected by the RT slope value, where steeper/larger slope values reflect (relatively) longer RTs in the SCD0 condition and thus indicate less expedient multicomponent behavior (Mückschel et al., 2014; Verbruggen et al., 2008). sNF-L concentrations between ~0.9 and ~8 pg/ml predicted RT differences of several hundred milliseconds, as reflected by the RT slope value (which ranged from ~0.1 to ~ −1: a value of 0 reflects no differences, while a slope of −1 reflects a 300 ms RT difference between the SCD0 and SCD300 condition). Given that (relatively) higher sNF-L concentrations were associated with steeper slopes, the data suggest that a high integrity of the neuronal cytoskeleton predicts a high expedience of multicomponent behavior.

Importantly, the neurophysiological data provided insights into the mechanism that mediates the effect of non-pathological, molecule-level variations in the integrity of the neuronal cytoskeleton on multicomponent behavior. It was shown that sNF-L levels were correlated with the parameter ω (i.e. the small world value) of theta oscillation-based networks and that the latter was also correlated with behavioral performance:

Specifically, the correlation between sNF-L levels and the slope of theta small-world values (ω) explained 56% of all observed theta ω variation within the sample. Given a correlation value of more than 0.5, it can be rather safely concluded that non-pathological variation in the integrity of the neuronal cytoskeleton is a major determinant of the neuronal network efficiency reflected by theta-associated small-world network properties. The small-world value of theta oscillations was generally larger in the SCD0 condition, which reflects a reduction in small-world characteristics/a more random network organization (Watts and Strogatz, 1998) and therefore a reduction in network efficiency, as compared to the SCD300 condition. It has been suggested that a small-world-like network architecture enables an efficient separation and functional integration of information, because this kind of network architecture shows a dense local interconnectivity and short average path length, thus linking nodes in a short and efficient way (Achard and Bullmore, 2007; Bassett and Bullmore, 2006; Bullmore and Sporns, 2009). It therefore seems that there is on average a more efficient separation and functional integration of information in the SCD300 condition than the SCD0 condition. Based on this, we hypothesized that the theta slope reflects or maybe even induces differences in task goal processing and the resulting behavior. In line with this, we found a strong positive correlation between the slope of the theta-associated ω

parameter and the slope of the SCD-RT function, which explained 59% of the behavioral variability: The less ω increases (i.e. loses it small-world like properties) in the SCD0 condition, the better (more efficient) multi-component behavior will be (as reflected by a flatter RT slope). This suggests that efficient multi-component behavior relates to the efficiency of information processing within theta-mediated oscillation networks. Given that the SCD300 condition enforces a step-by-step/serial processing, which is less likely to be found in the SCD0 condition, this further suggests that the small-world characteristics reflect demands on response selection processes and the load in the response selection bottleneck during cognitive control.

In order to further investigate the interrelation of neuronal cytoskeletal integrity, theta network efficiency and multicomponent behavior, we conducted a mediation analysis that allows to dissociate the direct and indirect effects of sNF-L variation onto our behavioral RT slope measure. The results revealed that there was not only a direct effect of sNF-L onto the RT slope, but also evidence for an indirect effect; i.e. that small-world network characteristics of theta oscillations mediated the effect of sNF-L levels on behavioral performance. Most noteworthy, the indirect mediation via theta oscillations was about 1.5 times larger than the direct effect of sNF-L on the behavioral slope measure. This strongly suggests that theta network efficiency might indeed provide a crucial functional link between molecular changes and multicomponent behavior and explain how even molecule-level variations in markers of neuronal cytoskeleton integrity may effectively modulate behavior in otherwise healthy, young adults. In this context, it should be noted that the observed effects seem to be quite specific, as we found no correlation of sNF-L and any other of the assessed neurophysiological measures. There were no correlations of sNF-L with attentional ERPs or small-world values (ω) within the alpha band. Most importantly, we also failed to find a correlation between sNF-L values and the amplitude of the fronto-central P3 ERP or total fronto-central theta power. In our sample, both measures (i.e. P3 ERP and fronto-central theta power) increased in the cognitively challenging SCD0 condition, which is well in line with previous studies in the stop-change paradigm (Mückschel et al., 2014; Stock et al., 2014a). In the context of the stop-change-paradigm, the P3 amplitude is thought to reflect both behavioral inhibition and change processes (Dippel and Beste, 2015), which matches the common finding that amplitudes are increased in case of intensified inhibitory control processes (Mückschel et al., 2017, 2014) and response inhibition efforts (Huster et al., 2013). The increased theta band power in the SCD0 condition most likely reflects a higher need for control (Cavanagh and Frank, 2014; Dippel and Beste, 2015) when the STOP and CHANGE stimuli are presented simultaneously so that subjects likely experience some degree of interference between the two task goals. But while P3 amplitudes and theta power have been shown to be modulated by many other factors such as dopamine, cytokines, or alcohol (Beste et al., 2015; Stock et al., 2014a, 2014b), this was definitively not the case in our study. Hence, there seems to be a functional dissociation between the sheer amplitude/power of a given neuronal activation and the efficiency with which information is being processed within a network. Only the latter seems to be modulated by the integrity of the neuronal cytoskeleton, but this functional nexus explains a staggering amount of behavioral performance variation, especially given that we only assessed healthy variation at the molecule level. This finding is of high relevance for research in clinical contexts using NF-L, in which the neurofilament parameter may be used for biomarker purposes since there are strong links between NF-L and the integrity of white matter structure as shown in studies on demyelinating diseases (Boesen et al., 2018; Khalil et al., 2018; Kuhle et al., 2016b, 2017; Melah et al., 2016). The current results show that even within a healthy control sample strong variations in behavioral or neuropsychological performance can be explained by tiny variations in sNF-L concentrations. Within a clinical context, it will therefore be necessary to consider the impact of physiological variations in more detail. For that it will be important to consider that the individual sNF-L profile may change considerably and may therefore reflect a variable 'state marker' that may affect neuropsychological performance. The variability and effects thereof need to be considered in studies examining the longitudinal profile of sNF-L variation together with longitudinal variations in cognitive performance. Future studies shall also consider other cognitive processes, including attentional selection functions. In the current study, attentional selection processes were not modulated by sNF-L concentrations. The possible reason for this is that attentional selection processes do not seem to be important for performance in this task (i.e. explain behavioral variations). Rather, it the integration of sensory information subsequent to attentional selection stages that is of importance (Gohil et al., 2017, 2016; Stock et al., 2017). This is also corroborated by data from studies populations with attentional deficits (Bluschke et al., 2018) and elderly people with otherwise diminished attentional capacities (Stock et al., 2016).

In summary, we found compelling evidence that slightest, non-pathological variations in the structural integrity of the neuronal cytoskeleton strongly modulate cognitive control processes that are important for everyday activities. We could further show that the architecture and efficiency of theta-oscillations networks (rather than signal strength/power) reflects a mechanism that establishes the relationship between structure and function. It hence seems that the efficiency/small-world architecture of theta oscillations might provide an important missing link which helps to explain and better understand how diffuse and seemingly miniscule changes in neuronal integrity may lead to reduced or even impaired cognitive functioning.

Acknowledgements

This work was supported by Grants from the Deutsche Forschungsgemeinschaft (DFG) BE4045/10-2 and SFB 940 project B8.

Appendix A. Supplementary data

Supplementary data related to this article can be found at https://doi.org/10.1016/j.neuroimage.2018.10.053.

References

Achard, S., Bullmore, E., 2007. Efficiency and cost of economical brain functional networks. PLoS Comput. Biol. 3, e17. https://doi.org/10.1371/journal.pcbi.0030017.

Bassett, D.S., Bullmore, E., 2006. Small-world brain networks. Neurosci. Rev. J. Bringing Neurobiol. Neurol. Psychiatry 12, 512–523. https://doi.org/10.1177/1073858406293182.

Beste, C., Kneiphof, J., Woitalla, D., 2015. Effects of fatigue on cognitive control in neurosarcoidosis. Eur. Neuropsychopharmacol. J. Eur. Coll. Neuropsychopharmacol. 25, 522–530. https://doi.org/10.1016/j.euroneuro.2015.01.012.

Bluschke, A., Gohil, K., Petzold, M., Roessner, V., Beste, C., 2018. Neural mechanisms underlying successful and deficient multi-component behavior in early adolescent ADHD. NeuroImage Clin 18, 533–542. https://doi.org/10.1016/j.nicl.2018.02.024.

Boesen, M.S., Jensen, P.E.H., Magyari, M., Born, A.P., Uldall, P.V., Blinkenberg, M., Sellebjerg, F., 2018. Increased cerebrospinal fluid chitinase 3-like 1 and neurofilament light chain in pediatric acquired demyelinating syndromes. Mult. Scler. Relat. Disord. 24, 175–183. https://doi.org/10.1016/j.msard.2018.05.017.

Brandt, V.C., Stock, A.-K., Münchau, A., Beste, C., 2017. Evidence for enhanced multi-component behaviour in Tourette syndrome - an EEG study. Sci. Rep. 7, 7722. https://doi.org/10.1038/s41598-017-08158-9.

Bullmore, E., Sporns, O., 2009. Complex brain networks: graph theoretical analysis of structural and functional systems. Nat. Rev. Neurosci. 10, 186–198. https://doi.org/10.1038/nrn2575.

Buzsáki, G., 2006. Rhythms of the Brain. Oxford Univ. Press, Oxford.

Buzsáki, G., Draguhn, A., 2004. Neuronal oscillations in cortical networks. Science 304, 1926–1929. https://doi.org/10.1126/science.1099745.

Cavanagh, J.F., Frank, M.J., 2014. Frontal theta as a mechanism for cognitive control. Trends Cognit. Sci. 18, 414–421. https://doi.org/10.1016/j.tics.2014.04.012.

Cohen, M.X., 2014. A neural microcircuit for cognitive conflict detection and signaling. Trends Neurosci. 37, 480–490. https://doi.org/10.1016/j.tins.2014.06.004.

Crick, F., Koch, C., 2003. A framework for consciousness. Nat. Neurosci. 6, 119.

Diamond, A., 2013. Executive functions. Annu. Rev. Psychol. 64, 135–168. https://doi.org/10.1146/annurev-psych-113011-143750.

Dippel, G., Beste, C., 2015. A causal role of the right inferior frontal cortex in implementing strategies for multi-component behaviour. Nat. Commun. 6, 6587. https://doi.org/10.1038/ncomms7587.

Disanto, G., Adiutori, R., Dobson, R., Martinelli, V., Dalla Costa, G., Runia, T., Evdoshenko, E., Thouvenot, E., Trojano, M., Norgren, N., Teunissen, C., Kappos, L., Giovannoni, G., Kuhle, J., International Clinically Isolated Syndrome Study Group, 2016. Serum neurofilament light chain levels are increased in patients with a clinically isolated syndrome. J. Neurol. Neurosurg. Psychiatry 87, 126–129. https://doi.org/10.1136/jnnp-2014-309690.

Disanto, G., Barro, C., Benkert, P., Naegelin, Y., Schädelin, S., Giardiello, A., Zecca, C., Blennow, K., Zetterberg, H., Leppert, D., Kappos, L., Gobbi, C., Kuhle, J., Swiss Multiple Sclerosis Cohort Study Group, 2017. serum neurofilament light: a biomarker of neuronal damage in multiple sclerosis. Ann. Neurol. 81, 857–870. https://doi.org/10.1002/ana.24954.

Duncan, J., 2010. The multiple-demand (MD) system of the primate brain: mental programs for intelligent behaviour. Trends Cognit. Sci. 14, 172–179. https://doi.org/10.1016/j.tics.2010.01.004.

Freunberger, R., Höller, Y., Griesmayr, B., Gruber, W., Sauseng, P., Klimesch, W., 2008. Functional similarities between the P1 component and alpha oscillations. Eur. J. Neurosci. 27, 2330–2340. https://doi.org/10.1111/j.1460-9568.2008.06190.x.

Gaiottino, J., Norgren, N., Dobson, R., Topping, J., Nissim, A., Malaspina, A., Bestwick, J.P., Monsch, A.U., Regeniter, A., Lindberg, R.L., Kappos, L., Leppert, D., Petzold, A., Giovannoni, G., Kuhle, J., 2013. Increased neurofilament light chain blood levels in neurodegenerative neurological diseases. PloS One 8, e75091. https://doi.org/10.1371/journal.pone.0075091.

Gisslén, M., Price, R.W., Andreasson, U., Norgren, N., Nilsson, S., Hagberg, L., Fuchs, D., Spudich, S., Blennow, K., Zetterberg, H., 2016. Corrigendum to: "Plasma concentration of the neurofilament light protein (NFL) is a biomarker of CNS injury in HIV infection: a cross-sectional study" [EBioMedicine 3 (216) 135-140]. EBioMedicine 7, 287–288. https://doi.org/10.1016/j.ebiom.2016.04.021.

Gohil, K., Bluschke, A., Roessner, V., Stock, A.-K., Beste, C., 2017. Sensory processes modulate differences in multi-component behavior and cognitive control between childhood and adulthood. Hum. Brain Mapp. 38, 4933–4945. https://doi.org/10.1002/hbm.23705.

Gohil, K., Hahne, A., Beste, C., 2016. Improvements of sensorimotor processes during action cascading associated with changes in sensory processing architecture-insights from sensory deprivation. Sci. Rep. 6, 28259. https://doi.org/10.1038/srep28259.

Gohil, K., Stock, A.-K., Beste, C., 2015. The importance of sensory integration processes for action cascading. Sci. Rep. 5, 9485. https://doi.org/10.1038/srep09485.

Gong, J., Luo, C., Chang, X., Zhang, R., Klugah-Brown, B., Guo, L., Xu, P., Yao, D., 2017. White matter connectivity pattern associate with characteristics of scalp EEG signals. Brain Topogr. 30, 797–809. https://doi.org/10.1007/s10548-017-0581-z.

Hayes, A.F., Montoya, A.K., Rockwood, N.J., 2017. The analysis of mechanisms and their contingencies: PROCESS versus structural equation modeling. Australas. Mark. J. AMJ 25, 76–81. https://doi.org/10.1016/j.ausmj.2017.02.001.

Herrmann, C.S., Knight, R.T., 2001. Mechanisms of human attention: event-related potentials and oscillations. Neurosci. Biobehav. Rev. 25, 465–476.

Hipp, J.F., Hawellek, D.J., Corbetta, M., Siegel, M., Engel, A.K., 2012. Large-scale cortical correlation structure of spontaneous oscillatory activity. Nat. Neurosci. 15, 884–890. https://doi.org/10.1038/nn.3101.

Huster, R.J., Enriquez-Geppert, S., Lavallee, C.F., Falkenstein, M., Herrmann, C.S., 2013. Electroencephalography of response inhibition tasks: functional networks and cognitive contributions. Int. J. Psychophysiol. Off. J. Int. Organ. Psychophysiol. 87, 217–233. https://doi.org/10.1016/j.ijpsycho.2012.08.001.

Kalisman, N., Silberberg, G., Markram, H., 2005. The neocortical microcircuit as a tabula rasa. Proc. Natl. Acad. Sci. U.S.A. 102, 880–885.

Kayser, J., Tenke, C.E., 2015. On the benefits of using surface Laplacian (current source density) methodology in electrophysiology. Int. J. Psychophysiol. Off. J. Int. Organ. Psychophysiol. 97, 171–173. https://doi.org/10.1016/j.ijpsycho.2015.06.001.

Khalil, M., Teunissen, C.E., Otto, M., Piehl, F., Sormani, M.P., Gattringer, T., Barro, C., Kappos, L., Comabella, M., Fazekas, F., Petzold, A., Blennow, K., Zetterberg, H., Kuhle, J., 2018. Neurofilaments as biomarkers in neurological disorders. Nat. Rev. Neurol. https://doi.org/10.1038/s41582-018-0058-z.

Kong, J., Tung, V.W., Aghajanian, J., Xu, Z., 1998. Antagonistic roles of neurofilament subunits NF-H and NF-M against NF-L in shaping dendritic arborization in spinal motor neurons. J. Cell Biol. 140, 1167–1176.

Kriz, J., Zhu, Q., Julien, J.P., Padjen, A.L., 2000. Electrophysiological properties of axons in mice lacking neurofilament subunit genes: disparity between conduction velocity and axon diameter in absence of NF-H. Brain Res. 885, 32–44.

Kuhle, J., Barro, C., Andreasson, U., Derfuss, T., Lindberg, R., Sandelius, Å., Liman, V., Norgren, N., Blennow, K., Zetterberg, H., 2016a. Comparison of three analytical platforms for quantification of the neurofilament light chain in blood samples: ELISA, electrochemiluminescence immunoassay and Simoa. Clin. Chem. Lab. Med. 54, 1655–1661. https://doi.org/10.1515/cclm-2015-1195.

Kuhle, J., Barro, C., Disanto, G., Mathias, A., Soneson, C., Bonnier, G., Yaldizli, Ö., Regeniter, A., Derfuss, T., Canales, M., Schluep, M., Du Pasquier, R., Krueger, G., Granziera, C., 2016b. Serum neurofilament light chain in early relapsing remitting MS is increased and correlates with CSF levels and with MRI measures of disease severity. Mult. Scler. Houndmills Basingstoke Engl. 22, 1550–1559. https://doi.org/10.1177/1352458515623365.

Kuhle, J., Barro, C., Disanto, G., Mathias, A., Soneson, C., Bonnier, G., Yaldizli, Ö., Regeniter, A., Derfuss, T., Canales, M., Schluep, M., Du Pasquier, R., Krueger, G., Granziera, C., 2016c. Serum neurofilament light chain in early relapsing remitting MS is increased and correlates with CSF levels and with MRI measures of disease severity. Mult. Scler. Houndmills Basingstoke Engl. 22, 1550–1559. https://doi.org/10.1177/1352458515623365.

Kuhle, J., Nourbakhsh, B., Grant, D., Morant, S., Barro, C., Yaldizli, Ö., Pelletier, D., Giovannoni, G., Waubant, E., Gnanapavan, S., 2017. Serum neurofilament is associated with progression of brain atrophy and disability in early MS. Neurology 88, 826–831. https://doi.org/10.1212/WNL.0000000000003653.

Lariviere, R.C., Julien, J.-P., 2004. Functions of intermediate filaments in neuronal development and disease. J. Neurobiol. 58, 131–148. https://doi.org/10.1002/neu.10270.

Lépinoux-Chambaud, C., Eyer, J., 2013. Review on intermediate filaments of the nervous system and their pathological alterations. Histochem. Cell Biol. 140, 13–22. https://doi.org/10.1007/s00418-013-1101-1.

Letzner, S., Güntürkün, O., Beste, C., 2017. How birds outperform humans in multi-component behavior. Curr. Biol. CB 27, R996–R998. https://doi.org/10.1016/j.cub.2017.07.056.

Logan, G.D., Cowan, W.B., Davis, K.A., 1984. On the ability to inhibit simple and choice reaction time responses: a model and a method. J. Exp. Psychol. Hum. Percept. Perform. 10, 276–291.

Luck, S.J., Kappenman, E.S. (Eds.), 2013. The Oxford Handbook of Event-related Potential Components. Oxford library of psychology. Oxford University Press, Oxford ; New York, NY.

Melah, K.E., Lu, S.Y.-F., Hoscheidt, S.M., Alexander, A.L., Adluru, N., Destiche, D.J., Carlsson, C.M., Zetterberg, H., Blennow, K., Okonkwo, O.C., Gleason, C.E., Dowling, N.M., Bratzke, L.C., Rowley, H.A., Sager, M.A., Asthana, S., Johnson, S.C., Bendlin, B.B., 2016. Cerebrospinal fluid markers of alzheimer's disease pathology and microglial activation are associated with altered white matter microstructure in asymptomatic adults at risk for alzheimer's disease. J. Alzheimers Dis. JAD 50, 873–886. https://doi.org/10.3233/JAD-150897.

Meyer, D.E., Kieras, D.E., 1997. A computational theory of executive cognitive processes and multiple-task performance: Part 1. Basic mechanisms. Psychol. Rev. 104, 3–65.

Miller, J., Ulrich, R., Rolke, B., 2009. On the optimality of serial and parallel processing in the psychological refractory period paradigm: effects of the distribution of stimulus onset asynchronies. Cognit. Psychol. 58, 273–310. https://doi.org/10.1016/j.cogpsych.2006.08.003.

Mückschel, M., Gohil, K., Ziemssen, T., Beste, C., 2017. The norepinephrine system and its relevance for multi-component behavior. Neuroimage 146, 1062–1070. https://doi.org/10.1016/j.neuroimage.2016.10.007.

Mückschel, M., Stock, A.-K., Beste, C., 2015. Different strategies, but indifferent strategy adaptation during action cascading. Sci. Rep. 5, 9992. https://doi.org/10.1038/srep09992.

Mückschel, M., Stock, A.-K., Beste, C., 2014. Psychophysiological mechanisms of interindividual differences in goal activation modes during action cascading, 1991 Cereb. Cortex N. Y. N 24, 2120–2129. https://doi.org/10.1093/cercor/bht066.

Nolte, G., Bai, O., Wheaton, L., Mari, Z., Vorbach, S., Hallett, M., 2004. Identifying true brain interaction from EEG data using the imaginary part of coherency. Clin. Neurophysiol. Off. J. Int. Fed. Clin. Neurophysiol. 115, 2292–2307. https://doi.org/10.1016/j.clinph.2004.04.029.

Nunez, P.L., Pilgreen, K.L., 1991. The spline-Laplacian in clinical neurophysiology: a method to improve EEG spatial resolution. J. Clin. Neurophysiol. Off. Publ. Am. Electroencephalogr. Soc. 8, 397–413.

Nunez, P.L., Silberstein, R.B., Shi, Z., Carpenter, M.R., Srinivasan, R., Tucker, D.M., Doran, S.M., Cadusch, P.J., Wijesinghe, R.S., 1999. EEG coherency II: experimental comparisons of multiple measures. Clin. Neurophysiol. 110, 469–486.

Nunez, P.L., Srinivasan, R., Westdorp, A.F., Wijesinghe, R.S., Tucker, D.M., Silberstein, R.B., Cadusch, P.J., 1997. EEG coherency: I: statistics, reference electrode, volume conduction, Laplacians, cortical imaging, and interpretation at multiple scales. Clin. Neurophysiol. 103, 499–515.

Peters, J.M., Taquet, M., Vega, C., Jeste, S.S., Fernández, I.S., Tan, J., Nelson, C.A., Sahin, M., Warfield, S.K., 2013. Brain functional networks in syndromic and non-syndromic autism: a graph theoretical study of EEG connectivity. BMC Med. 11, 54.

Petzold, A., Altintas, A., Andreoni, L., Bartos, A., Berthele, A., Blankenstein, M.A., Buee, L., Castellazzi, M., Cepok, S., Comabella, M., Constantinescu, C.S., Deisenhammer, F., Deniz, G., Erten, G., Espiño, M., Fainardi, E., Franciotta, D., Freedman, M.S., Giedraitis, V., Gilhus, N.E., Giovannoni, G., Glabinski, A., Grieb, P., Hartung, H.-P., Hemmer, B., Herukka, S.-K., Hintzen, R., Ingelsson, M., Jackson, S., Jacobsen, S., Jafari, N., Jalosinski, M., Jarius, S., Kapaki, E., Kieseier, B.C., Koel-Simmelink, M.J.A., Kornhuber, J., Kuhle, J., Kurzepa, J., Lalive, P.H., Lannfelt, L., Lehmensiek, V., Lewczuk, P., Livrea, P., Marnetto, F., Martino, D., Menge, T., Norgren, N., Papuć, E., Paraskevas, G.P., Pirttilä, T., Rajda, C., Rejdak, K., Ricny, J., Ripova, D., Rosengren, L., Ruggieri, M., Schraen, S., Shaw, G., Sindic, C., Siva, A., Stigbrand, T., Stonebridge, I., Topcular, B., Trojano, M., Tumani, H., Twaalfhoven, H.A.M., Vécsei, L., Van Pesch, V., Vanderstichele, H., Vedeler, C., Verbeek, M.M., Villar, L.M., Weissert, R., Wildemann, B., Yang, C., Yao, K., Teunissen, C.E., 2010. Neurofilament ELISA validation. J. Immunol. Methods 352, 23–31. https://doi.org/10.1016/j.jim.2009.09.014.

Pfurtscheller, G., Lopes da Silva, F.H., 1999. Event-related EEG/MEG synchronization and desynchronization: basic principles. Clin. Neurophysiol. Off. J. Int. Fed. Clin. Neurophysiol. 110, 1842–1857.

Racine, A.M., Merluzzi, A.P., Adluru, N., Norton, D., Koscik, R.L., Clark, L.R., Berman, S.E., Nicholas, C.R., Asthana, S., Alexander, A.L., Blennow, K., Zetterberg, H., Kim, W.H., Singh, V., Carlsson, C.M., Bendlin, B.B., Johnson, S.C., 2017. Association of longitudinal white matter degeneration and cerebrospinal fluid biomarkers of neurodegeneration, inflammation and Alzheimer's disease in late-middle-aged adults. Brain Imaging Behav. https://doi.org/10.1007/s11682-017-9732-9.

Roach, B.J., Mathalon, D.H., 2008. Event-related EEG time-frequency analysis: an overview of measures and an analysis of early gamma band phase locking in schizophrenia. Schizophr. Bull. 34, 907–926. https://doi.org/10.1093/schbul/sbn093.

Stam, C.J., van Straaten, E.C.W., 2012. The organization of physiological brain networks. Clin. Neurophysiol. 123, 1067–1087. https://doi.org/10.1016/j.clinph.2012.01.011.
Stock, A.-K., Arning, L., Epplen, J.T., Beste, C., 2014a. DRD1 and DRD2 genotypes modulate processing modes of goal activation processes during action cascading. J. Neurosci. Off. J. Soc. Neurosci. 34, 5335–5341. https://doi.org/10.1523/JNEUROSCI.5140-13.2014.
Stock, A.-K., Blaszkewicz, M., Beste, C., 2014b. Effects of binge drinking on action cascading processes: an EEG study. Arch. Toxicol. 88, 475–488. https://doi.org/10.1007/s00204-013-1109-2.
Stock, A.-K., Gohil, K., Beste, C., 2016. Age-related differences in task goal processing strategies during action cascading. Brain Struct. Funct. 221, 2767–2775. https://doi.org/10.1007/s00429-015-1071-2.
Stock, A.-K., Gohil, K., Huster, R.J., Beste, C., 2017. On the effects of multimodal information integration in multitasking. Sci. Rep. 7, 4927. https://doi.org/10.1038/s41598-017-04828-w.
Teipel, S., Grothe, M.J., Zhou, J., Sepulcre, J., Dyrba, M., Sorg, C., Babiloni, C., 2016. Measuring cortical connectivity in alzheimer's disease as a brain neural network pathology: toward clinical applications. J. Int. Neuropsychol. Soc. JINS 22, 138–163. https://doi.org/10.1017/S1355617715000995.
Telesford, Q.K., Joyce, K.E., Hayasaka, S., Burdette, J.H., Laurienti, P.J., 2011. The ubiquity of small-world networks. Brain Connect. 1, 367–375. https://doi.org/10.1089/brain.2011.0038.
Teunissen, C.E., Khalil, M., 2012. Neurofilaments as biomarkers in multiple sclerosis. Mult. Scler. Houndmills Basingstoke Engl. 18, 552–556. https://doi.org/10.1177/1352458512443092.
Vågberg, M., Norgren, N., Dring, A., Lindqvist, T., Birgander, R., Zetterberg, H., Svenningsson, A., 2015. Levels and Age Dependency of Neurofilament Light and Glial Fibrillary Acidic Protein in Healthy Individuals and Their Relation to the Brain Parenchymal Fraction. PloS One 10 e0135886. https://doi.org/10.1371/journal.pone.0135886.
Van Essen, D.C., 1997. A tension-based theory of morphogenesis and compact wiring in the central nervous system. Nature 385, 313.
Varela, F.J., 1995. Resonant cell assemblies: a new approach to cognitive functions and neuronal synchrony. Biol. Res. 28, 81–95.
Vecchio, F., Di Iorio, R., Miraglia, F., Granata, G., Romanello, R., Bramanti, P., Rossini, P.M., 2018. Transcranial direct current stimulation generates a transient increase of small-world in brain connectivity: an EEG graph theoretical analysis. Exp. Brain Res. 236, 1117–1127. https://doi.org/10.1007/s00221-018-5200-z.
Verbruggen, F., Schneider, D.W., Logan, G.D., 2008. How to stop and change a response: the role of goal activation in multitasking. J. Exp. Psychol. Hum. Percept. Perform. 34, 1212–1228. https://doi.org/10.1037/0096-1523.34.5.1212.
von der Malsburg, C., 1994. The correlation theory of brain function. New York. In: Domany, E., van Hemmen, J.L., Schulten, K. (Eds.), Models of Neural Networks. Springer, New York, NY, pp. 95–119. https://doi.org/10.1007/978-1-4612-4320-5_2.
Watts, D.J., Strogatz, S.H., 1998. Collective dynamics of “small-world” networks. Nature 393, 440–442. https://doi.org/10.1038/30918.
Wilson, D.H., Rissin, D.M., Kan, C.W., Fournier, D.R., Piech, T., Campbell, T.G., Meyer, R.E., Fishburn, M.W., Cabrera, C., Patel, P.P., Frew, E., Chen, Y., Chang, L., Ferrell, E.P., von Einem, V., McGuigan, W., Reinhardt, M., Sayer, H., Vielsack, C., Duffy, D.C., 2016. The Simoa HD-1 analyzer: a novel fully automated digital immunoassay analyzer with single-molecule sensitivity and multiplexing. J. Lab. Autom. 21, 533–547. https://doi.org/10.1177/2211068215589580.
Wolff, N., Zink, N., Stock, A.-K., Beste, C., 2017. On the relevance of the alpha frequency oscillation's small-world network architecture for cognitive flexibility. Sci. Rep. 7, 13910. https://doi.org/10.1038/s41598-017-14490-x.
Wu, C., Liu, Y., 2008. Queuing network modeling of the psychological refractory period (PRP). Psychol. Rev. 115, 913–954. https://doi.org/10.1037/a0013123.
Wu, T., Dufford, A.J., Egan, L.J., Mackie, M.-A., Chen, Cong, Yuan, C., Chen, Chao, Li, X., Liu, X., Hof, P.R., Fan, J., 2017. Hick-hyman law is mediated by the cognitive control network in the brain, 1991 Cereb. Cortex N. Y. N 1–16. https://doi.org/10.1093/cercor/bhx127.
Zetterberg, H., Smith, D.H., Blennow, K., 2013. Biomarkers of mild traumatic brain injury in cerebrospinal fluid and blood. Nat. Rev. Neurol. 9, 201–210. https://doi.org/10.1038/nrneurol.2013.9.
Zink, N., Stock, A.-K., Colzato, L., Beste, C., 2018. Evidence for a neural dual-process account for adverse effects of cognitive control. Brain Struct. Funct. 223, 3347–3363. https://doi.org/10.1007/s00429-018-1694-1.